PAPER

Polar pattern formation: hydrodynamic coupling of driven filaments†

Volker Schaller,[a] Christoph Weber,[b] Erwin Frey[b] and Andreas R. Bausch*[a]

How order can emerge spontaneously from a disordered system has always fascinated scientists from numerous disciplines. Especially in active systems like flocks animals, self-propelled microorganisms or the cytoskeleton, a unifying understanding of the pattern formation remains elusive. This is attributed to the inherent complexity of most model systems that prevents a thorough identification of the fundamental mechanisms that are responsible for the intriguing self-organizing phenomena in active systems. Here we show that long ranged hydrodynamic interactions play a crucial role in the pattern forming mechanisms in the high density motility assay, a precisely controllable minimal model system consisting of highly concentrated filaments that are driven on the nanoscale. Stability and size of the patterns depend on long ranged hydrodynamic interactions that are self-induced by the coherently moving filaments. The hydrodynamic interactions not only influence the spatial and temporal scale of the patterns but also affect the dynamics of a particular cluster in close proximity to confining boundaries or other surrounding clusters.

Introduction

It is by now well known that maintaining a system far from thermal equilibrium by external constraints induces a plethora of spatio-temporal patterns. Active systems like flocks of animals, self-propelled microorganisms or the cytoskeleton constitute yet another intriguing class of non-equilibrium systems.[1–13] Here locally generated internal forces together with interactions between the constituents are the cause for remarkable self-organization processes that lead to structures as diverse as animal groups on the move,[7,14] swarming microorganisms[4–6] or aster-like structures in cytoskeletal systems.[9,10] Theoretical approaches to model such systems range from micro- or mesoscopic studies[15–22] to generic hydrodynamic theories.[23–25] Despite these approaches, a unifying understanding of this material class of active suspensions is still elusive. Primarily this can be attributed to the lack of adequate model systems that allow for a precise identification of the underlying ordering principles.[26] In this context, the recently introduced high density motility assay has proven to be a model system ideally suited for examining the organizing principles in active suspensions.[12,13]

It was found that above a critical filament density, clusters and density waves of coherently moving filaments start to form. The emergence of these structures was traced back to local short range interactions. Yet, these interactions alone do not suffice to explain the remarkable stability of the patterns.[13]

To elucidate this problem, we now address the role of long ranged interactions.

We show that stability and size of the patterns formed in the high density motility assay depend on long ranged hydrodynamic interactions that are self-induced by the coherently moving filaments. This can be seen by observing (1) the emergence of patterns from an isotropic phase, (2) the interaction between colliding clusters and (3) the dynamics of clusters within confinements that are produced by microcontact imprinting.

Results and discussion

In a motility assay at low concentrations of F-actin, individual filaments move randomly and cross each other frequently. The increase in the filament concentration above a critical concentration c^* results in the emergence of clusters of coherently moving filaments.[13] The higher the density, the larger the average size of these clusters gets. While the directional persistence of small clusters is poorly developed, larger clusters are less prone to changes in their direction of motion. At even higher densities above c^{**}, the orientational persistence is high enough, so that density fluctuations within the clusters can grow and density waves start to evolve. Apart from the orientational fluctuations both patterns, the density waves and the clusters, show a remarkable structural integrity. Individual clusters are stable for several minutes and density waves can proceed for up to 45 min. Neither clusters nor density waves get destroyed or

[a]*Lehrstuhl für Zellbiophysik E 27, Technische Universität München, James-Franck-Straße 1, 85748 Garching, Germany. E-mail: abausch@ph.tum.de*
[b]*Arnold Sommerfeld Center for Theoretical Physics and CeNS, Department of Physics, Ludwig-Maximilians-Universität, Theresienstr. 37, 80333 München, Germany*
† Electronic supplementary information (ESI) available: Additional data/pictures and video captions as described in the main text. See DOI: 10.1039/c0sm01063d

dissolve instantaneously. For decorrelation and destruction of clusters, splay or bending instabilities are mainly responsible.[13]

1. Synchronization of emergent patterns

One key aspect in understanding the dynamical properties and stability of these structures lies in the observation of their emergence. In order to visualize the emergence of the density waves, samples were prepared in the absence of ATP at filament densities above c^{**}. Under this condition the filaments bind to the motors in the rigor state in an isotropic and homogenous fashion, where no orientational preference of the filaments is observable. Upon addition of ATP, molecular motors are activated and filaments start to move in an uncoordinated fashion. Local interactions result in the emergence of small polar zones that span the width of a few filaments only and exhibit small wavelength oscillations (Fig. 1) This is similar to theoretical model systems where the constituents interact through inelastic collisions.[27] The successive coordination and synchronization of extended coherently moving areas result in the formation of domains which grow larger and move with increasingly greater persistence (Fig. 1 and Video S1 in the ESI†). Once a sufficient directional persistence is reached, density waves appear. They are the result of density fluctuations, which are not damped any more, if a sufficiently high orientational persistence is provided.

Thus the observed pattern forming process relies on the successive synchronization of ordered patches that are much more than an average filament length apart. Neither this synchronization process nor the remarkable stability of the evolving structures can be explained by purely short ranged interactions alone. Rather, this suggests the presence of a medium to long ranged interaction. While electrostatic interactions are effectively screened in the electrolyte solutions, hydrodynamic interactions are the most promising candidate.

2. Sensibility against external fluid flow

Despite being crafted to the surface by molecular motors, actin filaments in a motility assay are highly sensible to external fluid flow. If subjected to a laminar shear flow with a flow velocity in the order of the filament velocity, the filaments orient and move alongside the fluid flow (Fig. 2a and b). After cessation of the
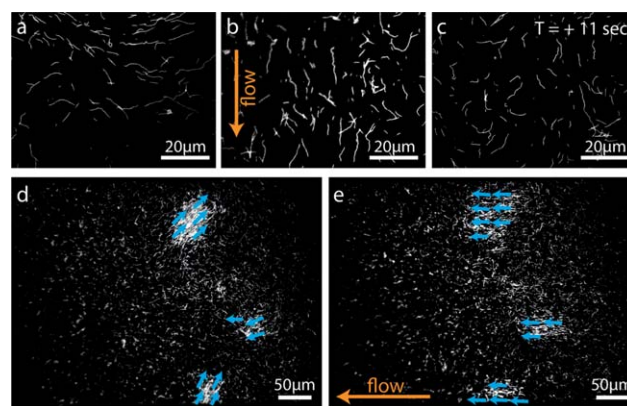

Fig. 2 Orientation alongside external flow fields. A motility assay experiment is subjected to a hydrodynamic flow field directed along the arrow in images (b) and (e). In the low density phase (images (a)–(c)), before being subjected to an external flow field, individual filaments perform random walks with only a minor directional preference (a). When the external flow is applied, the filaments get oriented alongside the flow (b). After cessation of the flow and a certain relaxation time T in the order of 10 s, the filaments resume their random walk and the directional bias due to the flow alignment gradually vanishes (c). In the cluster phase, individual clusters move uncorrelated (d). When subjected to a flow field, the clusters orient alongside the flow (e). The filament density for (a)–(c) was set to $\rho = 2$ µm^{-2} for (a)–(c) and to $\rho = 7$ µm^{-2} for (d) and (e).

flow, filaments gradually loose their orientation and resume their persistent random walk (Fig. 2c).

Clusters of coherently moving filaments are even more sensible to externally imposed fluid flows. They already reorient alongside the flow if subjected to flow velocities that are not sufficient to turn individual filaments (Fig. 2d and f and Video S2 in the ESI†). Similar to individual filaments they gradually loose the directional bias once the flow is stopped. The time after which the clusters have lost the directional bias due to the external flow depends on the magnitude of the flow velocity: the higher the velocity of the external fluid flow, the better the alignment alongside the flow and the longer it takes for the clusters to loose the externally imposed direction.

In the high density motility assay flow fields are self-induced by the coherently moving structures. Despite the hydrodynamic
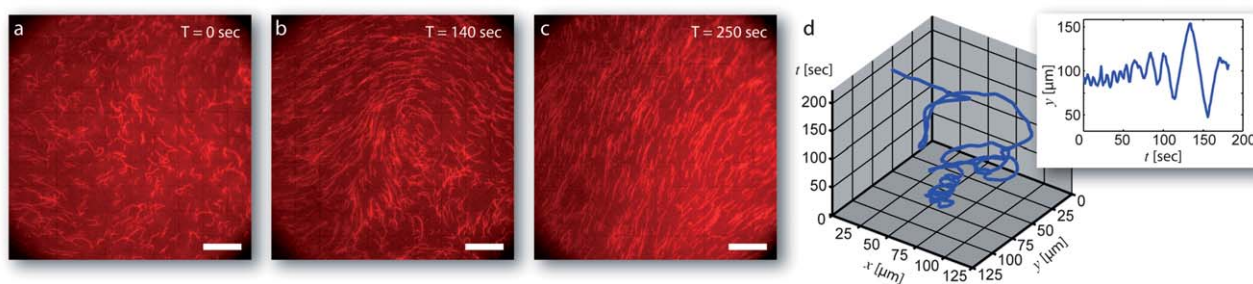

Fig. 1 Emergence of collective motion. Images (a)–(c) illustrate the gradual formation of ordered structures starting from a polar and homogeneous basic state. After the addition of ATP, the filaments move in an oscillatory manner on circular trajectories with a growing radius as can be seen in (d), where the trajectory of an individual filament is shown. The orientational instability results in the gradual emergence of ordered zones that successively coarsen. The further the ordering has progressed, the more space is cleared for further binding of filaments to the motor proteins at the surface and initially only partly bound filaments can bind fully. Consequently, the apparent filament length at the surface increases concomitantly with increasing order. The filament density amounts to $\rho = 21$ µm^{-2} and the scale bar is 20 µm.

drag individual filament can generate is limited in reach to several nanometers,[28] large coherently moving structures like density waves generate a stable fluid flow that lately extends throughout the entire flow chamber.

3. Hydrodynamic interactions between clusters

These flow fields naturally influence the dynamics in the high density motility assay, as it becomes manifest if coherently moving structures interact with adjacent patterns. A gradual increase in the filament density not only results in an increased average size of the clusters, but also in their more frequent occurrence. The enhanced cluster density leads to more frequent collisions between clusters, in the course of which the clusters reorient and reorganize their shape.

During collisions clusters approach each other only up to a minimal distance d_{min}, which is of the order of a filament length. Reorganization and reorientation of the clusters during collisions take place *before* the cluster's margins physically touch. As a consequence, a depletion zone with a thickness of d_{min} forms that is given by the minimal distance between two colliding clusters (Fig. 3 and Video S3 in the ESI†). Being short range in nature, simple hard core repulsion does not suffice to describe this scattering behavior; rather, it can be attributed to the hydrodynamic coupling of the flow fields of interacting clusters. The existence of the depletion zone prevents colliding clusters from merging with one another in a coarsening process and thus adds to the enormous stability of individual clusters.

4. Impact of a boundary on the pattern formation

It can be expected that interactions with hard walls lead to similar behavior: if a cluster scatters at a solid wall, it should only approach the wall up to a minimal distance d_{min} and a depletion layer should form. To address this, the diameter of active regions was systematically reduced down to 50 μm with the help of micropatterning techniques (Fig. 4a). The boundary between the active and passive region is characterized by a sharp margin (Fig. 4c). Filaments are only propelled within the active region and are repelled and have to turn around at the boundaries. Provided that the active region is sufficiently large, the confinement does not change the overall behavior of the system and the same density dependent phenomenology is observed. Above the critical density $c*$ clusters evolve inside the active region (Fig. 4b) and similar to the case without confinement, clusters grow larger with increasing density. If the clusters are large enough, their
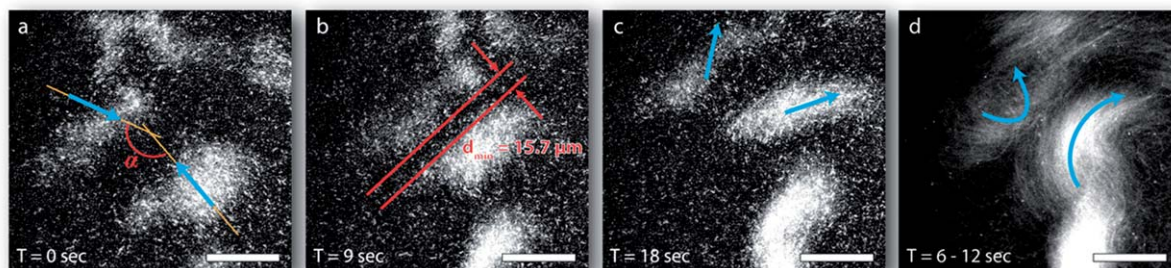

Fig. 3 Dynamics of interacting clusters. Images (a)–(c) show a typical scattering process of two interacting clusters. The arrows denote the direction of motion of the clusters. Even for scatter events with an interaction angle close to $\alpha = 180°$, the formation of a depletion layer with a thickness of d_{min} in between the interacting clusters is observed (b). This can also be seen in the time overlay in image (d) where the trajectories of the interacting clusters are visualized (arrows). The filament density was adjusted to $\rho = 14$ μm^{-2} and the scale bar is 50 μm.
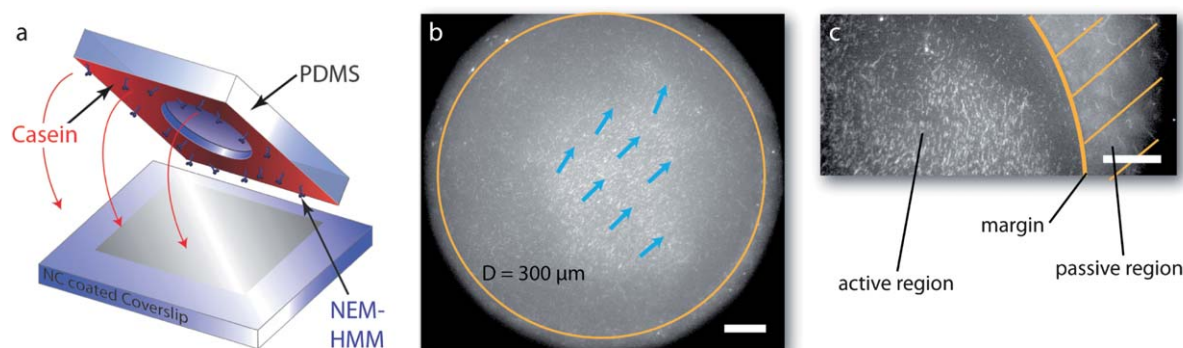

Fig. 4 Microcontact imprinting technique. Image (a) shows a schematic representation of the used microcontact imprinting technique, with the help of which arbitrary boundaries with a diameter down to 50 μm can be designed. To selectively passivate distinct regions, a PDMS stamp treated with Casein and HMM motor proteins in the rigor state (NEM–HMM) is placed on the coverslip (for further details, see materials and methods). This procedure results in an active region and a passive region made up of filamentous actin bound to rigor HMM (c). The boundary of the two regions is characterized by a sharp margin. In (b), a cluster moving in a circular boundary is shown (see Video S3 in the ESI†). The filament density is set to $\rho = 14$ μm^{-2} and the scale bar is 50 μm.

directional persistence gets higher than the diameter of the confinement. Unavoidably, this leads to multiple scattering events of the coherently moving structure with the boundary in the course of which the cluster successively explores the entire active region (Video S4 in the ESI†).

The interference with the confinement has severe consequences on the emergence of density waves. In contrast to the case without confinement, no density waves could be found below
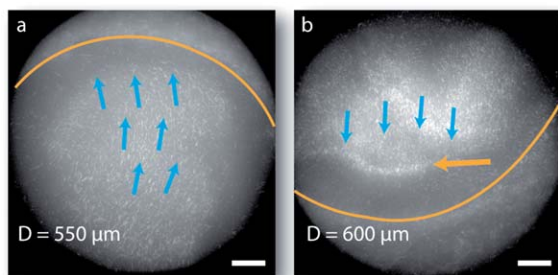

Fig. 5 Boundaries suppress the formation of density waves. For too small active regions the mean free path between boundary encounters is not sufficient for the density waves to evolve. In this case, the filaments move inhomogenous clusters as can be seen in (a) for a circular active region with a diameter of $D = 550$ μm. Above a diameter of $D = 600$ μm enough maneuvering space is given and density in homogeneities (long arrow) can develop before they get destroyed by collisions with the boundary. In (a) and (b), the direction of motion is indicated by arrows and the boundary of the active region is marked by a line; the scale bar is 50 μm and the filament density is set to $\rho = 18$ μm^{-2}.

a confinement diameter of 550 ± 25 μm (Fig. 5). This is consistent with the observation of the emergence of density waves in the high density motility assay without confinement: the density fluctuations need a minimal orientational persistence and hence a minimal mean free path to evolve into stable density modulations.[13] In confinement, the mean free path is set by the dimensions of the active regions, as density modulations are destroyed during interactions with the boundary (Fig. 6a–c and Video S5 in the ESI†). Below a confinement diameter of 550 ± 25 μm scattering events occur too often for stable density modulations to evolve.

Importantly, if geometry confines the high density motility assay into structures smaller than 75 ± 25 μm, no coherently moving patterns evolve at all. Already small clusters cannot evolve in such confining geometries as their persistence length of the movement is too large. Only in a sufficiently large active region, enough maneuvering space is given to allow for the synchronization process and hence the formation of stable patterns. This is equivalent to the notion that the hydrodynamic interactions need to be fully developed to stabilize the emerging structures.

5. Hydrodynamic interactions with confining boundaries

Besides, the usage of boundaries on the μm scale allows for a systematic investigation of the influence of hydrodynamic interactions. Similar to the occurrence of a depletion zone during two-cluster interactions, clusters turn around already before reaching the boundary, while individual filaments do this at the
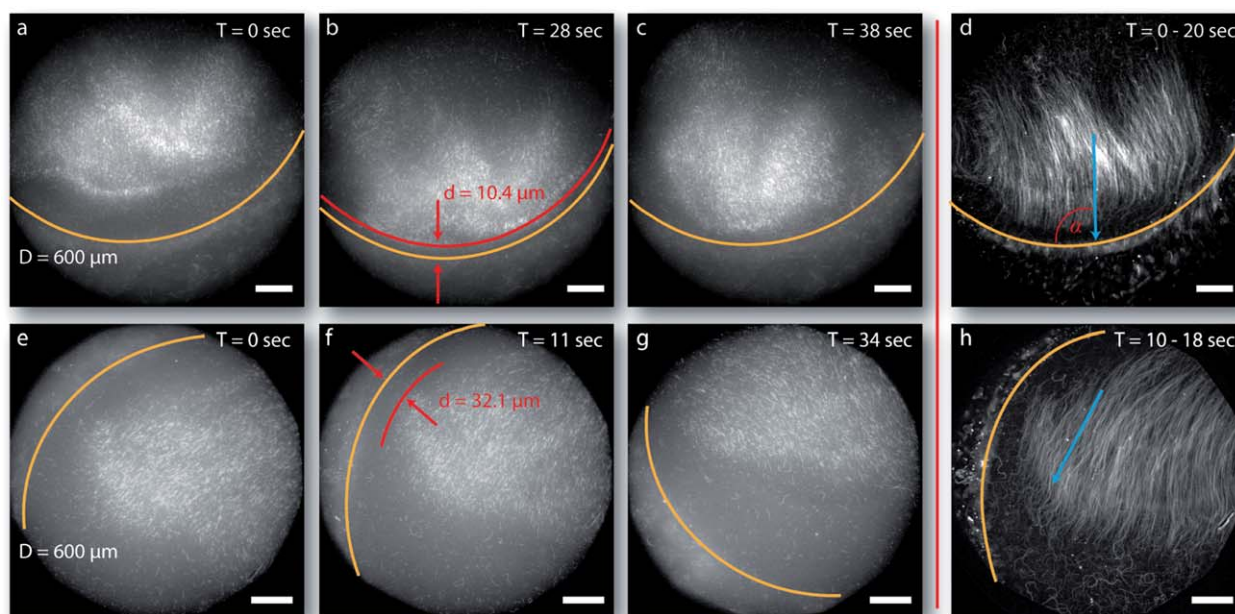

Fig. 6 Formation of a depletion layer during interactions with boundaries. The images (a)–(c) and (e)–(g) illustrate a sequence of snapshots for two scattering events of clusters with the boundary (line); (d) and (h) are the corresponding time overlays and the arrows denote the direction of motion. Whereas (a)–(d) feature an intersection angle close to $\alpha = 90°$ (d), the image series (e)–(h) shows the cluster–wall interaction for an interaction angle close to $\alpha = 0°$. In both cases, for $\alpha = 90°$ and $\alpha = 0°$, a depletion layer is formed and the clusters already turn before physically touching the boundary (b and f). The thickness of the depletion layer and the change in the cluster morphology depend on the angle of intersection: angles close to 90° lead to a minimal depletion layer of ~10 μm and a complete reorganization of the clusters; small angles yield larger depletion layers in the order of 30 μm. The filament density is set to $\rho = 20$ μm^{-2} and the scale bar is 50 μm.

boundary itself. Depending on the intersection angle, clusters are repelled at distances of up to 30 μm from the wall. Angles close to 90° result in shallow depletion zones and major changes in the cluster morphology (Fig. 6a–d and Video S5 in the ESI†) while small angles lead to larger depletion zones with minor reorientations of the clusters (Fig. 6e–h). Still the overall cluster integrity is not disturbed—demonstrating once again the enormous stability of the cluster, which is again attributed to the shielding through a self-induced flow field since other long ranged cohesive interactions are assuredly absent.

The occurrence of an angle dependent minimal cluster-to-wall distance d_{min} during such scattering events is a direct proof for the existence of long ranged interactions in the system. Purely short ranged interaction can neither account for the occurrence of a depletion zone nor for the observed angular dependence.

This is reminiscent of theoretical work on solid objects moving parallel to a wall.[29] Here the objects are likewise subjected to a torque that increases with decreasing distance from the wall. In the motility assay, this torque leads to a rotation of the direction of movement of the clusters and their deflection from the wall.

For high filament densities, 90° collisions are unlikely to develop since the mean free path for individual structures is too small and interactions with boundaries predominantly occur at shallow interaction angles. This 'guiding effect' of the wall can be utilized to tune the movement of the structures, as can be seen in Fig. S1 in the ESI†, where circular boundaries induce persistent swirling motions. In this case, the confinement reduces the movement of the swirls center that limits the stability of spontaneously formed swirls in the high density motility assay without confinement.[13]

Conclusions

The described pattern formation mechanisms—from the synchronization of extended patterns to the occurrence of depletion zones in interactions with interfering structures—emphasize the importance of long ranged interactions in the high density motility assay. While the emergence of collective motion can be explained by predominately short ranged interactions,[13] short ranged interactions alone can neither account for the long-term stability of the patterns nor for the intriguing behavior when collectively moving structures interact with their environment. In the high density motility assay long ranged interactions are self-induced by the collectively moving filaments. In the ordered phase, the short range decay of the hydrodynamic flow fields of individual filaments adds up to a significant contribution with a large number of coherently moving filaments.

The cooperative hydrodynamic interaction of many filaments not only leads to the observed self-stabilization of even small clusters and to the long range interaction between individual clusters or clusters and hard walls, but also sets the spatial and temporal scales of the patterns. It is thus a key mechanism for the formation of the coherent structures in this system.

In contrast to bacteria swarms, the filament clusters in the high density motility assay need not swim through the fluid but are propelled by the motor proteins. Conceptually, this yields a force monopole flow field that is much longer ranged than the flow fields for low-Re swimmers.[30] Nevertheless, these findings support the mechanisms identified for the pattern formation mechanisms in

suspensions of active microparticles such as bacteria,[31] where coherent structures likewise evolve on length scales considerably exceeding the size of the individual constituents.[3–6]

The identified interplay of local weak alignment interactions and long range hydrodynamics makes the high density motility assay ideal for manipulating and steering the self-organization process and the emerging patterns over several orders of magnitude. The demonstrated steering by local flow or micro-patterning opens up the possibility for the wellcontrolled design of patterns in active fluids.

Materials and methods

G-actin is obtained from rabbit skeletal muscle following ref. 32, and is stored and polymerized into filaments as described before.[33] Solutions were prepared by dissolving lyophilized G-actin in deionized water and dialysing against fresh G-Buffer (2 mM Tris, 0.2 mM ATP, 0.2 mM $CaCl_2$, 0.2 mM DTT and 0.005% NaN_3) at 4 °C for 24 h. Actin polymerization was initiated by adding one-tenth of the sample volume of a tenfold concentrated F-buffer (20 mM Tris, 20 mM $MgCl_2$, 2 mM $CaCl_2$, 2 mM DTT and 1 M KCl). For fluorescence microscopy, reporter filaments are fluorescently labelled at a ratio of labelled to unlabeled filaments ranging from 1 : 200 to 1 : 500. If not stated otherwise they are stabilized with Alexa-Fluor-488-phalloidin (Invitrogen) at a ratio of 1 : 4. Unlabeled filaments are stabilized with phalloidin (Sigma) likewise at a ratio of 1 : 4. Once polymerized, actin was used within 5 days. HMM is prepared from myosin II obtained from rabbit skeletal muscle following a standardized protocol.[34] Rigor HMM (NEM–HMM) is prepared by modifying HMM with N-ethyl-maleimide.[35]

Sample preparation

Flow chambers were prepared with an overall volume of 45 μl. Prior to each experiment, a 50 μl actin dilution (1–20 μM monomeric actin) was prepared by gently mixing labelled and unlabelled actin filaments with Assay Buffer (25 mM Imidazolhydrochlorid pH 7.4; 25 mM KCl; 4 mM $MgCl_2$; 1 mM EGTA; 1 mM DTT). To prevent oxidation of the fluorophore, a standard antioxidant buffer supplement (Glucose–Oxidase, Sigma, 2 mg; Catalase, Fluka, 0.5 mg; and DTT) was used. The flow chamber was incubated with HMM diluted in Assay Buffer. After the incubation of HMM surfaces are passified with BSA (Sigma). Excess ATP is added to rule out ATP depletion effects, which is verified by a constant filament-speed of 4.8 μm s^{-1} for the entire period of observation (up to 45 min).

Externally imposed flow fields

The flow fields were generated by attaching a syringe to the flow chamber. During flow pulses, the flow rate was (6 ± 2) μl s^{-1}. The area cross-section of the flow chamber was 2 mm^2 with a height of 0.5 mm and a width of 4 mm. The velocity of the flow fields was checked by evaluating the velocity of confluent particles close to the surface.

Microcontact imprinting

To functionalize the surface on the μm scale, a microcontact imprinting technique based on poly(dimethylsiloxane) (PDMS) stamps was used. The fabrication of the stamps follows the procedure for rapid prototyping of microfluidic devices.[36] More specifically, the design of the desired structure is printed in high resolution (3000 dpi) on a transparency which is used as a mask to expose SU-8 50 positive photoresist (Microchem). After developing, the SU-8 structure serves as a master for the casting of PDMS, which is poured onto the master as a liquid. PDMS was cured overnight at 70 °C.

After being removed from the master, the PDMS replica of the structure is cleaned with isopropanol (Roth) and plasma oxidized. To selectively passivate distinct regions of the coverslip, the stamp is wetted for 3 min with a mixture of NEM–HMM and 1 mg ml^{-1} Casein diluted in Assay Buffer and then surface dried for 30 s. Subsequently, it is placed on the coverslip. After an incubation time of 3 min it is removed and the motility assay is prepared as described above.

Image acquisition

All data were acquired on a Zeiss Axiovert 200 inverted microscope with a ×100 oil objective (numerical aperture: 1.4) or a ×40 oil objective (numerical aperture: 1.3) and a Leica DMI 6000 inverted microscope with a ×40 oil objective (numerical aperture: 1.25). Images were captured at a rate of one image per 117 ms with a charge-coupled device camera (C4880-80, Hamamatsu) attached *via* a 0.4 (Zeiss) or 0.35 (Leica) camera mount. Image acquisition and storage were carried out with the image processing software 'OpenBox'.[37] For the images displayed in Fig. 2 and 3, background subtraction and contrast enhancement were carried out with ImageJ. The velocity fields displayed in Fig. 2 were calculated with a PIV routine written in MATLAB.

Acknowledgements

References

1 A. Kudrolli, G. Lumay, D. Volfson and L. S. Tsimring, *Phys. Rev. Lett.*, 2008, **100**, 058001.
2 V. Narayan, S. Ramaswamy and N. Menon, *Science*, 2007, **317**, 105–108.
3 T. J. Pedley and J. O. Kessler, *Annu. Rev. Fluid Mech.*, 1992, **24**, 313.
4 C. Dombrowski, L. Cisneros, S. Chatkaew, R. E. Goldstein and J. O. Kessler, *Phys. Rev. Lett.*, 2004, **93**, 098103.
5 I. H. Riedel, K. Kruse and J. Howard, *Science*, 2005, **309**, 300–303.
6 A. Sokolov, I. S. Aranson, J. O. Kessler and R. E. Goldstein, *Phys. Rev. Lett.*, 2007, **98**, 158102.
7 A. J. W. Ward, D. J. T. Sumpter, L. D. Couzin, P. J. B. Hart and J. Krause, *Proc. Natl. Acad. Sci. U. S. A.*, 2008, **105**, 6948.
8 M. Moussaid, S. Garnier, G. Theraulaz and D. Helbing, *Top. Cogn. Sci.*, 2009, **1**, 469.
9 F. J. Nedelec, T. Surrey, A. C. Maggs and S. Leibler, *Nature*, 1997, **389**, 305.
10 F. Backouche, L. Haviv, D. Groswasser and A. Bernheim-Groswasser, *Phys. Biol.*, 2006, **3**, 264.
11 D. Smith, F. Ziebert, D. Humphrey, C. Duggan, M. Steinbeck, W. Zimmermann and J. Käs, *Biophys. J.*, 2007, **93**, 4445.
12 T. Butt, T. Mufti, A. Humayun, P. B. Rosenthal, S. Khan and J. E. Molloy, *J. Biol. Chem.*, 2009, **285**, 4964.
13 V. Schaller, C. Weber, C. Semmrich, E. Frey and A. R. Bausch, *Nature*, 2010, **467**, 73.
14 I. D. Couzin, J. Krause, N. R. Franks and S. A. Levin, *Nature*, 2005, **433**, 513.
15 T. Vicsek, A. Czirok, E. Benjacob, I. Cohen and O. Shochet, *Phys. Rev. Lett.*, 1995, **75**, 1226–1229.
16 H. Chate, F. Ginelli, G. Gregoire and F. Raynaud, *Phys. Rev. E: Stat. Phys., Plasmas, Fluids, Relat. Interdiscip. Top.*, 2008, **77**, 046113.
17 P. Kraikivski, R. Lipowsky and J. Kierfeld, *Phys. Rev. Lett.*, 2006, **96**, 258103.
18 I. S. Aranson and L. S. Tsimring, *Phys. Rev. E: Stat. Phys., Plasmas, Fluids, Relat. Interdiscip. Top.*, 2005, **71**, 050901.
19 F. Peruani, A. Deutsch and M. Bär, *Phys. Rev. E: Stat. Phys., Plasmas, Fluids, Relat. Interdiscip. Top.*, 2006, **74**, 030904.
20 E. Bertin, M. Droz and G. Gregoire, *Phys. Rev. E: Stat. Phys., Plasmas, Fluids, Relat. Interdiscip. Top.*, 2006, **74**, 022101.
21 A. Baskaran and M. C. Marchetti, *Proc. Natl. Acad. Sci. U. S. A.*, 2009, **106**, 15567.
22 S. Mishra, A. Baskaran and M. C. Marchetti, *Phys. Rev. E: Stat. Phys., Plasmas, Fluids, Relat. Interdiscip. Top.*, 2010, **81**, 061916.
23 R. A. Simha and S. Ramaswamy, *Phys. Rev. Lett.*, 2002, **89**, 058101.
24 K. Kruse, J. F. Joanny, F. Julicher, J. Prost and K. Sekimoto, *Phys. Rev. Lett.*, 2004, **92**, 078101.
25 J. F. Joanny, F. Julicher, K. Kruse and J. Prost, *New J. Phys.*, 2007, **9**, 422.
26 J. Toner, Y. H. Tu and S. Ramaswamy, *Ann. Phys.*, 2005, **318**, 170.
27 D. Grossman, I. S. Aranson and E. Ben Jacob, *New J. Phys.*, 2008, **10**, 023036.
28 A. J. Hunt, F. Gittes and J. Howard, *Biophys. J.*, 1994, **67**, 766.
29 A. J. Goldman, R. G. Cox and H. Brenner, *Chem. Eng. Sci.*, 1967, **22**, 653.
30 K. Drescher, R. E. Goldstein, N. Michel, M. Polin and I. Tuval, *Phys. Rev. Lett.*, 2010, **105**, 168101.
31 V. Gyrya, I. S. Aranson, L. V. Berlyand and D. Karpeev, *Bull. Math. Biol.*, 2010, **72**, 148.
32 J. A. Spudich and S. Watt, *J. Biol. Chem.*, 1971, **246**, 4866.
33 Y. Luan, O. Lieleg, B. Wagner and A. R. Bausch, *Biophys. J.*, 2008, **94**, 688.
34 J. Uhde, M. Keller, E. Sackmann, A. Parmeggiani and E. Frey, *Phys. Rev. Lett.*, 2004, **93**, 268101.
35 R. L. Meeusen and W. Z. Cande, *J. Cell Biol.*, 1979, **82**, 57.
36 J. C. McDonald and G. M. Whitesides, *Acc. Chem. Res.*, 2002, **35**, 491.
37 J. Schilling, E. Sackmann and A. R. Bausch, *Rev. Sci. Instrum.*, 2004, **75**, 2822.